




Ion stopping force from Bohmian mechanics

P. L. Grande ^{*} and R. C. Fadanelli 

*Ion Implantation Laboratory, Instituto de Física, Universidade Federal do Rio Grande do Sul (UFRGS),
Av. Bento Gonçalves 9500, 91501-970 Porto Alegre, Rio Grande do Sul, Brazil*

F. Vuković , A. Niggas , and R. A. Wilhelm [†]

TU Wien, Institute of Applied Physics, Wiedner Hauptstrasse 8-10, 1040 Vienna, Austria

 (Received 20 May 2025; revised 10 August 2025; accepted 6 January 2026; published 17 February 2026)

We employed Bohmian mechanics to solve the equations of motion for a charged particle traveling in a free electron gas. Quantum effects are accounted for by including the Bohm quantum-mechanical potential Q , which depends on the electronic density, in the typical classical description. Our approach provides a computationally efficient alternative to traditional quantum calculations for determining the electronic stopping force of charged particles in matter. We use this framework to investigate the stopping of fast protons and slow highly charged xenon ions in the free electron gas. For highly charged ions, we predict the stopping force as a function of the projectile charge exchange.

DOI: [10.1103/7plq-xskx](https://doi.org/10.1103/7plq-xskx)

I. INTRODUCTION

Bohmian mechanics [1], also known as the de Broglie-Bohm theory or pilot-wave theory, is an interpretation of quantum mechanics that posits the existence of a guiding wave along with particles. In this framework, particles are governed by the Schrödinger equation, and the guiding wave determines their trajectories. This method allows straightforward quantization of classical calculations by adding an extra potential energy term: the quantum Bohm potential Q [1]. Following its original formulation by de Broglie and its systematic development by Bohm in the early 1950s [1,2], the formalism has been placed on solid conceptual and mathematical foundations, as discussed in several seminal monographs and reviews [3–5].

Beyond its foundational aspects, Bohmian mechanics has been extensively applied as a practical, analytical, and numerical tool in a wide range of physical contexts. Notable applications include quantum scattering and tunneling phenomena, molecular and chemical reaction dynamics, quantum chaos, nanoscale transport, and strong-field processes, where Bohmian trajectories provide valuable physical insight into quantum fluxes, interference patterns, and momentum transfer mechanisms [6–8]. In recent years, the approach has also been extended to open quantum systems and many-particle dynamics, further broadening its applicability [9]. A more general statistical formulation of quantum mechanics is discussed elsewhere [10,11].

Unfortunately, the quantum Bohm potential can be highly complex and computationally expensive to calculate, especially for many-body systems. This restricts its use to mean-field independent-particle models where the single particle density describes all particles [12]. The calculation of the quantum Bohm potential requires the second derivative of the electron density. Minor numerical uncertainties in the density can be amplified when taking these derivatives, leading to instability and inaccuracies in the resulting potential and trajectories. Here, we propose a stable method for expressing the quantum Bohm potential, suitable for calculating the stopping force. We demonstrate the utility of this approach by calculating the electronic stopping force encountered by charged particles in solids and two-dimensional (2D) materials from first principles, and in a computationally efficient manner.

The stopping force of ions in matter is a crucial parameter in both the low-energy [13,14] and the high-energy [15] regimes. At low projectile energies, it is relevant for both semiconductor device fabrication and nuclear materials design, where phenomena such as the depth of implantation and the damage of the lattice must be known and controlled to high precision [16,17]. At higher energies, the stopping force is used to determine ion penetration depths of ions in matter, which is an intrinsic aspect of ion-beam analysis [18] and ion-beam therapy [15,19]. Generalizing classical calculations using the Bohm quantum potential is also relevant in plasma physics [12,20] for a more accurate description of the interactions inside the plasma, where quantum effects may be significant [12]. The quantum potential is able to incorporate these effects into classical trajectories, providing a more comprehensive understanding of the plasma behavior and the interaction of particles within it.

To apply the Bohm potential in the context of ion-atom and ion-surface interactions, we use a statistical ensemble of all possible ion trajectories and then it gives rise to a nonlinear Schrödinger equation (NLSE) [21]. This equation describes

^{*}Contact author: grande@if.ufrgs.br

[†]Contact author: wilhelm@iap.tuwien.ac.at

stationary scattering states that are necessary to accurately model the (quantum) stopping force and ion screening in a dense electronic environment like a surface. We apply this method to study the energy loss of slow, highly charged Xe ions caused by the valence electrons of graphene. Recent measurements and *ab initio* time-dependent density functional theory (TDDFT) calculations showed a considerable energy loss, which depends on the incident charge state q_{in} and on the outgoing charge state q_{out} [22,23]. However, typically TDDFT calculations cannot treat many-body effects such as inter- and intraatomic Auger transitions [24–26]. Therefore, they could not fully describe the energy loss as a function of projectile charge exchange ($\Delta q = q_{\text{in}} - q_{\text{out}}$).

In contrast, classical simulations offer an excellent and cost-effective method to enhance [27] and expand stopping-force calculations to include charge exchange effects for slow highly charged ions interacting with 2D membranes [28]. They can be further quantized by adding the appropriate Bohm quantum potential. Full expressions are provided here for the free electron gas (FEG) system and for the binary theory of stopping [29]. Moreover, analytical expressions for the Bohm quantum potential were obtained for bare ions at high velocities.

While Bohmian mechanics offers an alternative view of nature and is now being put to experimental test [30], numerical challenges have long limited its practical application. Our results demonstrate that it can indeed enable quantum calculations with significantly reduced computational cost, highlighting its potential for broader application, particularly in scenarios where standard numerical methods are inadequate. The following section will describe the theoretical procedure to retrieve the Bohm quantum potential of an FEG quantum system, which features the valence electron of a solid or 2D membrane. Atomic units will be used throughout the paper unless otherwise stated.

II. THEORETICAL PROCEDURE

We first consider the stopping of a pointlike charged particle, Z_1 , traveling toward a classical FEG with an undisturbed electron density n or plasmon frequency $\omega_p = \sqrt{4\pi n}$. In the Z_1 reference frame, a front of electrons of density n and velocity \vec{v} are scattered by Z_1 . This scattering is described by a screened potential $V(\vec{r})$, where \vec{r} is the position vector between an electron and Z_1 . The classical trajectories are denoted by $\vec{r}_{\text{cl}}(t, \vec{b})$ for electrons coming from “the left to the right” with an impact parameter \vec{b} . The stationary density of electrons is then

$$\rho(\vec{r}) = nv \int dt \int d^2b \delta^{(3)}(\vec{r} - \vec{r}_{\text{cl}}(t, \vec{b})). \quad (1)$$

The induced electron density $n_{\text{ind}}(\vec{r}) = \rho(\vec{r}) - n$ then acts as a force \vec{F}_{ind} on the projectile. This retarding force is then the so-called “stopping force” [31],

$$\frac{dE}{dx} = -\frac{1}{v} \vec{F}_{\text{ind}} \cdot \vec{v}. \quad (2)$$

According to Bohmian Mechanics, classical calculations can be transformed into fully quantum-mechanical ones by

adding the quantum potential $Q(\vec{r})$ as

$$Q = -\frac{1}{2A} \nabla^2 A, \quad (3)$$

where A is the magnitude of the wave function, or simply $\sqrt{\rho}$ for a system of independent electrons. Thus, the Schrödinger equation is fully recovered by the Hamilton-Jacobi formalism [32]. From Eq. (1), the spherically averaged density can be determined by (see Appendix B)

$$A^2 = n \sqrt{1 - \frac{V}{E} - \frac{Q}{E}}, \quad (4)$$

where $E = v^2/2$. A microcanonical ensemble can obtain the same expression (see the Supplemental Material [33]). The quantum potential Q can then be determined from the density (A^2) as

$$Q = E \left(1 - \frac{A^4}{n^2} \right) - V(r). \quad (5)$$

With the definition of the Bohm quantum potential, Eq. (5) originates the following radial NLSE:

$$-\frac{1}{2} \left(\frac{d^2 A}{dr^2} + \frac{2}{r} \frac{dA}{dr} \right) = \left(E \left(1 - \frac{A^4}{n^2} \right) - V(r) \right) A. \quad (6)$$

This NLSE is the main result of the present work. The total potential to be used in classical calculations is

$$V_{\text{tot}} = V + Q = E \left(1 - \frac{A^4}{n^2} \right), \quad (7)$$

which gives quantum features to classical calculations. Furthermore, Eq. (6) gives the same solutions as the original Schrödinger equation for central problems and angular momentum $\ell = 0$. Solutions for other angular momenta can be obtained by incorporating the centrifugal potential $\ell(\ell + 1)/(2r^2)$.

Within Bohmian mechanics, the Newton-like equation containing the quantum force is derived rather than postulated. Its dynamical equivalence to the guiding equation holds only when the particle velocity is initially given by the gradient of the phase of the wave function. In the present work, this condition is explicitly assumed in Eq. (1) for an incident plane wave, which satisfies the continuity equation.

For small Z and large v , analytical solutions to Eq. (6) can be obtained for small perturbations in the density (see the Supplemental Material [33]). For example, for the Yukawa potential $V(r) = -\frac{Z_1}{r} \exp(-\alpha r)$, the perturbative solution results in an induced density

$$n_{\text{ind}} = 4 \frac{\omega_p^2 Z_1}{4\pi r} \frac{\exp(-\alpha r) - \exp(-2vr)}{4v^2 - \alpha^2}, \quad (8)$$

which agrees with the one obtained for the Nagy potential at $v \gg v_F$ (Fermi velocity $v_F = 1.919/r_s$) [34], with a Wigner-Seitz radius $r_s = (3n/4\pi)^{1/3}$ and using $\alpha = \omega_p/v$. Moreover, the induced density from Eq. (8) can be integrated to obtain the total induced charge, and the final expression yields the same full quantum-mechanical results as those in Ref. [35].

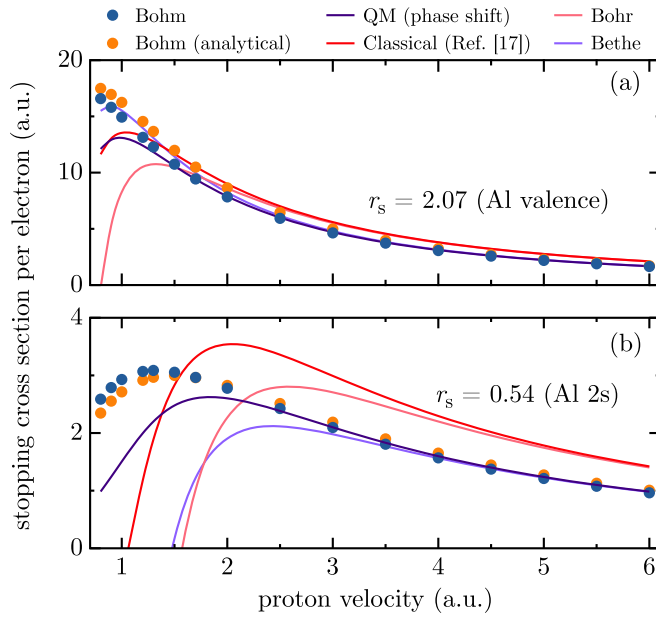


FIG. 1. The stopping cross section per electron of protons slowing down in an FEG with $r_s = 2.07$ [panel (a)], which features the Al valence electrons and $r_s = 0.54$ featuring the Al $2s$ shell [panel (b)]. The solid curves correspond to full classical and quantum calculations using the Yukawa potential and the screening length v/ω_p as well as to standard Bohr and Bethe stopping formulas. The symbols present the results based on Bohm trajectories. The ordinate values are calculated from the stopping force $\frac{dE}{dx}$ divided by the electron density $N = 1/(4\pi/3r_s^3)$ for the corresponding r_s values.

III. RESULTS AND DISCUSSIONS

Traditionally, perturbations in the electron gas (or electron density) caused by a moving charged particle have been treated linearly [36]. Here, we used the total ion-electron potential described in Eq. (7) and calculated the Bohmian trajectories for an FEG with different densities n or $r_s = (3n/4\pi)^{1/3}$. The stopping force was obtained from the induced force or transport cross section according to Ref. [29]:

$$\frac{dE}{dx} = \begin{cases} nv_F v \sigma(v_F), & \text{if } v \ll v_F, \\ nv^2 \sigma(v), & \text{if } v \gg v_F, \end{cases} \quad (9)$$

where σ is the effective transport cross section [37]

$$\sigma_{tr}^{\text{eff}} = -2\pi \frac{Z_1}{v^2} \int_0^\infty db \sin \Theta(b), \quad (10)$$

or the momentum-transfer cross section

$$\sigma_{tr} = 2\pi \int_0^\infty b db (1 - \cos \Theta(b)). \quad (11)$$

The first one is valid only for bare ions and works better at high projectile energies, whereas the second one is more appropriate for low projectile velocities [38].

A. Stopping at high projectile velocities

First, we consider a simple case of a fast proton in an aluminiumlike FEG. Figure 1(a) presents the calculated stopping force as a function of proton velocity for an FEG with

$r_s = 2.07$, which corresponds to the valence electron density of aluminium. Classical calculations (red solid line), based on Eq. (10) and employing a Yukawa potential with a screening length v/ω_p , are obtained by solving the classical orbit equation. These data are consistent with Bohr's stopping theory (rose solid line) at high projectile velocities, as recently confirmed for FEG systems [27]. It should be noted that for $v < 1$, the assumptions of unidirectional projectile trajectories [see Eq. (1)] and the use of v/ω_p as a screening length become no longer valid.

The classical trajectories were then recalculated from Newton's equation of motion by incorporating the quantum potential according to Eq. (7), yielding the Bohmian trajectories shown as blue points. We find good agreement with the full quantum-mechanical calculations using the phase-shift method [29,37] (green) for $v > 1.5$ and also with the Bethe formula (violet) at high projectile velocities. There are small discrepancies between the Bohmian trajectories and the phase-shift calculation due to the spherical averaging used to derive Eq. (6).

The best method to solve this NLSE is described in Appendix A. The analytical solution of this equation for small values of Z_1/v [33] was also used to recalculate the Bohmian trajectories (indicated by orange points). The agreement is only good at much higher projectile velocities. Overall, the primary effect of adding the quantum potential at high projectile energies is to truncate the interaction potential at distances comparable to the de Broglie wavelength of the incoming electron (in the center-of-mass (CM) system). In the Supplemental Material [33], we demonstrated that the analytical solution of the quantum potential yields the Bethe formula correctly at high projectile velocities.

Figure 1(b) illustrates the same scenario but for a much denser FEG system, whose plasmon energy corresponds to the binding energy of the Al $2s$ shell. Here, the discrepancy between classical and quantum stopping-force calculations becomes more pronounced. This is primarily due to enhanced electron screening, which intensifies the deviation between the two approaches. In this high-density regime, the Bohmian method is able to overcome the limitations of traditional classical calculations. The Bohmian results show excellent agreement with the quantum stopping forces obtained from phase-shift calculations for projectile velocities $v > 2$.

Strictly speaking, the results shown in Fig. 1 are valid for $v \gg v_F$, but they can be extended to lower velocities by incorporating kinematic (or shell) corrections, as described in Ref. [29]. This procedure for $r_s = 2.07$ was applied and is illustrated in Fig. 2. For this purpose, we used a velocity-dependent screening length of Nagy and Bergara [39] normalized by the Friedel sum rule [35]. Figure 2 also includes the TDDFT calculations for $r_s = 2.07$ and Al experimental data from Ref. [40]. The agreement between the TDDFT and Bohmian results, as well as the experimental data, is very good at low energies, indicating that both methods adequately describe H stopping by the Al valence electrons. At higher energies, the stopping due to the contribution of Al inner-shell electrons becomes significant, which can be taken into account by using an average of FEG stopping powers as displayed in the Supplemental Material [33]. We observe here that the Bohmian calculations yield even

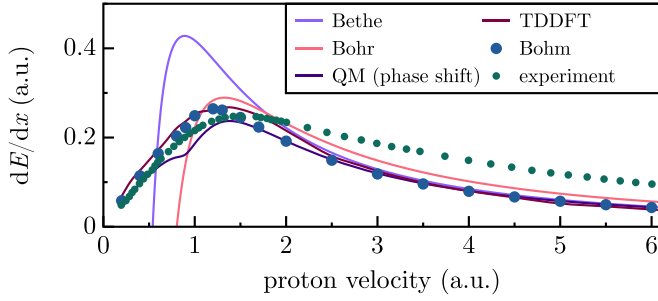


FIG. 2. The stopping force of protons in Al. The calculated values are as in Fig. 1(a), but including the electron initial velocities and velocity-dependent screening—see text. The blue dots are based on Bohm trajectories, and the red line corresponds to full TDDFT calculations from Ref. [40]. Experimental results from Ref. [40] are also added for reference.

better agreement with experiment than the quantum-mechanical (QM) phase-shift calculation. The spherical averaging used here implies a microcanonical ensemble, which seems to be more appropriate than the one behind the phase-shift calculations.

B. Stopping at low projectile velocities—highly charged ions

Next, we consider the case of slow, highly charged ions impinging on graphene. For this, a good description of the electron-ion interaction potential is required. Here, we consider the time-dependent potential (TDPot) model, developed to calculate the charge exchange and energy loss of slow, highly charged ions that impinge on 2D materials [41]. It gives a suitable description of the interatomic potential between the highly charged ions and the target atoms, and can be tuned for collisions between the incoming ion and the valence electrons of the membrane.

The TDPot model agrees with the experimental data [28,42] at low projectile velocities, but does not give the electronic energy loss for cases without charge exchange. To summarize, this model has three distinct stages: (1) neutralization of the ion and formation of a hollow atom prior to impact with the target [43], (2) stabilization of the ion during impact mediated by ultrafast interatomic Coulomb decay (ICD) [26], and (3) postimpact electron removal via Auger transitions. Nuclear energy loss arises from collisions between projectile and target atoms, and inelastic energy loss can be calculated from the time variation of the potential. In the limiting case of no charge exchange, the incoming and outgoing potentials are similar, resulting in an unphysically vanishing inelastic energy loss.

By assuming an FEG with electron density from the sp^2 and π orbitals of graphene, the inelastic energy loss can be calculated using Bohmian mechanics. Bohmian trajectories were then calculated using Eq. (7) and used to determine the stopping force following Eqs. (9) and (11) for $v \ll v_F$. The energy loss was calculated using 3.3 \AA for the thickness of graphene and $r_s = 1.5$, which is consistent with the areal density of the valence electron of $4 \times 3.8 \times 10^{15} \text{ cm}^{-2}$. The potential $V(r)$ used in Eq. (6) is described in terms of the projectile charge, the number of core, stabilized, and captured electrons as derived in Ref. [41] and depicted in Appendix C.

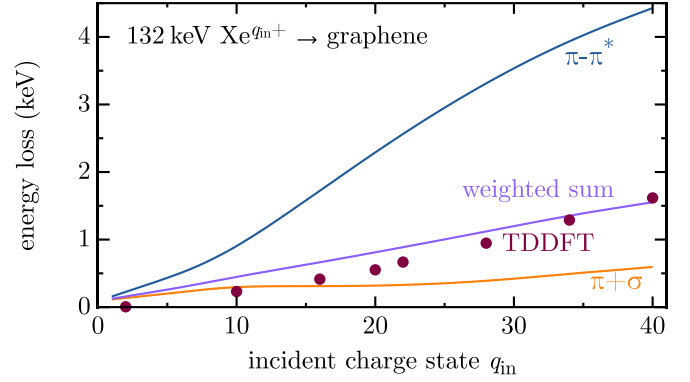


FIG. 3. Bohm calculations of the electronic energy loss of 132 keV Xe ions as a function of the incident charge state q_{in} on graphene, considering different projectile-electron screenings due to $\pi - \pi^*$ transitions with 5 eV and $\sigma + \pi$ plasmon excitations with 15 eV [44], are presented. The present results are compared with TDDFT calculations from Refs. [22,47].

Within the TDPot model, $V(r)$ remains neutral until the ion has left the target. Nevertheless, the graphene electrons can still dynamically screen the interaction. As such, we consider excitation energies of 4.7–6.8 eV for $\pi - \pi^*$ transitions and 15–27 eV for $\sigma + \pi$ plasmons [44–46]. We use this approach to screen the projectile-electron Coulombic interaction, as proposed and applied in the binary theory of electronic stopping by Sigmund [29]. Plasmon excitation contributions of 20% and 80% [46] were assumed for $\pi - \pi^*$ and $\sigma + \pi$ transitions, respectively.

Figure 3 presents the mean energy loss of 132 keV $Xe^{q_{in}+}$ ions in graphene as a function of the incident charge state q_{in} . The results are compared with TDDFT calculations from Ref. [22], which employ a cut-off radius of $R = 0.5$ to regularize the Coulomb singularity at the ion nucleus [47]. Individual contributions to the mean energy loss from the $\pi - \pi^*$ and $\sigma + \pi$ plasmons (see figure caption) are shown separately. Remarkably, the combined result closely matches the TDDFT predictions, considering the latter’s sensitivity to the choice of cut-off radius. This agreement is notable, given that the present approach is significantly simpler, computationally less demanding, and that approximations made in Ref. [22]. It is noted that the Bohm-based calculations presented here employ a constant, q_{in} -dependent potential with $N_{stab} = 0$ and $N_{cap} = 0$ (cf. Appendix C), in accordance with the assumptions made in the TDDFT calculations to enable direct comparison. In the following, the three-phase potential described above will be employed for comparison with experimental data.

A comparison of our Bohm calculations with the experimental energy loss data for 114 keV Xe^{26+} as a function of the outgoing charge q_{out} is provided in Fig. 4(b). The experimental data are obtained for ions transmitted through graphene and scattered into the forward direction within $\pm 0.1^\circ$. The obtained outgoing charge state spectrum is given in Fig. 4(a). The bimodal q_{out} distribution arises from the ion-beam sampling different regions of the graphene membrane during the experiment. As outlined in Ref. [48], inhomogeneities in sample thickness due to hydrocarbon contaminations can lead to

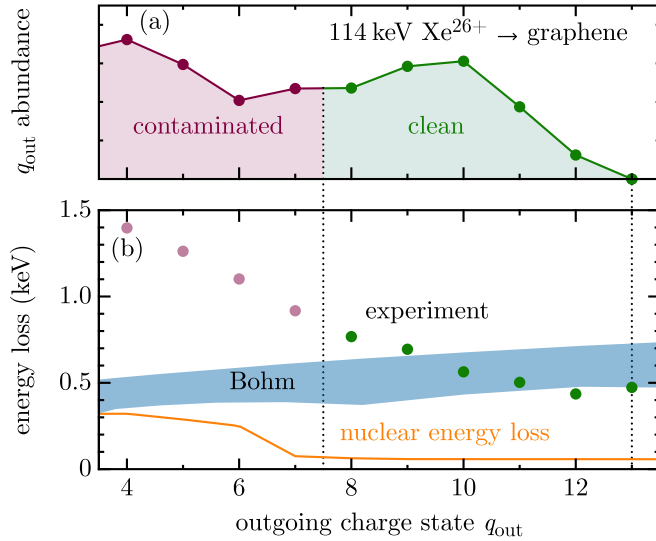


FIG. 4. (a) Measured outgoing charge state abundance of 114 keV Xe^{26+} ions through graphene. The part attributed to transmission through clean graphene is colored in green, while thicker and contaminated parts of the sample lead to the red-colored distribution. (b) The blue-colored area gives the electronic energy loss of 114 keV Xe^{26+} ions on graphene as a function of the outgoing charge state q_{out} for different energies of $\pi - \pi^*$ transitions (4.7–6.8 eV) and $\sigma - \pi$ plasmon energies (15–27 eV) from the Bohm model. The solid orange line corresponds to the calculated nuclear energy loss for an angular acceptance of 0.1° and other parameters described in the text. The dots are the experimentally determined mean energy loss. The colors and dotted vertical lines, as well as the solid line, are to indicate the data valid for clean graphene and to guide the eye, respectively.

larger charge exchange and energy loss. The higher charge state distribution peaking at $q_{\text{out}} \sim 9.5$ can be attributed to clean monolayer graphene, and the mean outgoing charge is very well comparable to the value estimated from previous work [49].

In our calculations, we now allow $N_{\text{stab}} \neq 0$ and $N_{\text{cap}} \neq 0$ in Eq. (C1) for TDPot-like as outlined in Ref. [41]. We apply this charge-dependent potential to Eq. (6), thereby transforming the classical calculations into fully quantum-mechanical ones.

The quantum potential Q was determined from Eq. (6) within the adiabatic approximation. Calculating the particle trajectory and acting forces using Newton's equations of motion with V_{tot} from Eq. (7) and using the Verlet algorithm within the Bohmian calculations yields electronic stopping.

The quantum potential Q was determined from Eq. (6) within the adiabatic approximation. In this approach, it is assumed that the A in Eq. (6) adjusts instantaneously to the slower motion of the Xe ion. Once the total potential energy V_{tot} was obtained from Eq. (7), the motion of each particle was followed by solving Newton's equations of motion. In practical terms, this means that the position and velocity of each particle were updated step by step according to the forces derived from the total potential. The numerical integration was performed using the velocity Verlet algorithm, which is widely used in molecular dynamics simulations because it provides high numerical stability and accurately conserves

total energy over long simulation times. The electronic stopping power was then determined using Eq. (11). This calculation was based on the momentum transfer to the projectile due to collisions with electrons of graphene. The final electronic stopping power values were averaged over a large set of independent trajectories, each initiated with slightly different impact parameters. For the nuclear stopping, we used standard TDPot calculations [see orange in Fig. 4(b)]. It increases with Δq , considering target atom excitations (with excitation parameters $\alpha = 10$ and $\beta = 2v$ as outlined in Ref. [41]). It represents the maximum possible nuclear energy loss and is significantly smaller than the experimental data for the acceptance angle of 0.1° in the forward direction. The electronic stopping of the Bohm model shows an increase in energy loss with q_{out} . The results are shown as a blue-colored region to account for the uncertainty of the graphene plasmon energies used to screen the ion-electron interaction. Within the range of outgoing charge states observed for clean graphene in the experiment ($q_{\text{out}} = 8$ –13), the Bohm calculations reproduce the experimental energy-loss data well. We can conclude that the energy loss for a straightforward transmission direction is dominated by electronic stopping [50] and that the total value can be well calculated by the presented Bohm model.

IV. CONCLUSIONS

We have introduced a method to determine the ion stopping force by converting classical calculations into quantum-mechanical ones using Bohmian mechanics. We solve classical equations of motion for a quantum-mechanical potential V_{tot} , which in turn depends on the quantum-mechanical Bohm potential Q . The latter is evaluated from the solid's electron density. This approach offers a computationally efficient alternative to traditional quantum-mechanical calculations for determining the electronic stopping force. We used this method to calculate the stopping of protons in aluminum (for FEGs featuring 2s and valence electrons) and highly charged ions in graphene. This demonstrates the approach's practical applicability and effectiveness. Furthermore, we predict the electronic stopping force of slow ions as a function of the ion charge exchange. The applicability of our approach to fast and slow ions, including highly dynamic charge-exchange scenarios, provides a robust foundation for quantum-mechanical stopping-force calculations in previously unfeasible complex cases. This enables quantitative predictions of ion-beam modifications in nuclear materials, plasma technology, and modern semiconductor and quantum materials.

ACKNOWLEDGMENTS

Part of this study was financed by the Coordenação de Aperfeiçoamento de Pessoal de Nível Superior—Brazil (CAPES)—Finance Code 001, by FINEP, by Conselho Nacional de Desenvolvimento Científico e Tecnológico (CNPq) Process No. 403722/2023-3, and by Instituto Nacional de Engenharia de Superfícies (INES) Project No. 465423/2014-0. This research was funded in whole or in part by the Austrian Science Fund (FWF) (Grants DOI 10.55776/Y1174 and DOI 10.55776/P36264).

DATA AVAILABILITY

The data that support the findings of this article are openly available [51].

APPENDIX A: NLSE—NUMERICAL SOLUTION

The Bohm quantum potential [Eq. (3)] considering m_e as the electron mass and \hbar is given by

$$\nabla^2 A = -\frac{2m_e}{\hbar^2} Q(\vec{r})A(\vec{r}). \quad (\text{A1})$$

In this work, we use an approach described in Ref. [52], in which the Green's function is given by

$$G(\vec{r} - \vec{r}') = \frac{1}{|\vec{r} - \vec{r}'|}, \quad (\text{A2})$$

using the so-called Dirichlet boundary conditions, namely, $G(r \rightarrow \infty) = 0$.

Since $A(r \rightarrow \infty, \theta, \phi) = \sqrt{n}$, we have

$$A(\vec{r}) - \sqrt{n} = \frac{m_e}{2\pi\hbar^2} \int Q(\vec{r}')A(\vec{r}')G(\vec{r} - \vec{r}')d^3r', \quad (\text{A3})$$

$$A(\vec{r}) = \sqrt{n} + \frac{m_e}{2\pi\hbar^2} \int \frac{Q(\vec{r}')A(\vec{r}')}{|\vec{r} - \vec{r}'|} d^3r'. \quad (\text{A4})$$

Since, in this work, both Q and A are obtained from central potentials, we can rewrite Eq. (A4) as

$$A(r) = \sqrt{n} + \frac{2m_e}{\hbar^2 r} \int_0^r dr' r'^2 Q(r')A(r') + \frac{2m_e}{\hbar^2} \int_r^\infty dr' r' Q(r')A(r'). \quad (\text{A5})$$

This integral equation was solved iteratively, starting with the initial guess $A = \sqrt{n}$, and typically converged within a few steps.

APPENDIX B: RELATION BETWEEN ELECTRON DENSITY A^2 AND THE TOTAL POTENTIAL

The spherical averaged density can be determined from Eq. (1) and is written as

$$\begin{aligned} \rho(r) = A^2 &= \frac{2nv}{4\pi r^2} \int d^2b \frac{1}{r_{cl}(r, b)} \\ &= \frac{n}{r^2} \int bdb \left(1 - \frac{V_{\text{tot}}}{E} - \frac{b^2}{r^2}\right)^{-\frac{1}{2}} \\ &= n \int_0^{\sqrt{1 - \frac{V_{\text{tot}}}{E}}} pdp \left(1 - \frac{V_{\text{tot}}}{E} - p^2\right)^{-\frac{1}{2}}, \quad (\text{B1}) \end{aligned}$$

for $V_{\text{tot}} < 0$ as for the present cases. Therefore,

$$A^2 = n\sqrt{1 - \frac{V_{\text{tot}}}{E}}, \quad (\text{B2})$$

with $V_{\text{tot}} = V + Q$.

APPENDIX C: ELECTRON-ION POTENTIAL

Here, we describe the model for the time-dependent electron-ion potential at $t = 0$ used in the FEG-Bohm calculations. The input of this model is the time-dependent number of electrons bound to the projectile $N_1(t) = N_{\text{core}} + N_{\text{cap}}(t) + N_{\text{stab}}(t)$, which is separated into three parts. The first one is the number of unchanged or frozen electrons during the collision (N_{core}), which populate the inner shells of the ion. The second part is the number of captured electrons (N_{cap}) from the graphene into highly excited Rydberg states in the ion. Part of these electrons (N_{stab}) are stabilized via Auger decay or extremely fast ICD [26].

The time-dependent interaction potential used here is given by (atomic units are used throughout this appendix)

$$\begin{aligned} V(R, t) &= -\frac{(N_{\text{core}} + N_{\text{stab}}(t))}{R} \\ &\times \phi\left(\frac{R}{a_1((N_{\text{core}} + N_{\text{stab}}(t)), N_2)}\right) \\ &- \frac{N_{\text{cap}}(t)}{R} \phi_{\text{hollow}}^{\text{cap}}(R, r_0) \\ &- \frac{(Z_1 - N_{\text{core}} - N_{\text{stab}}(t) - N_{\text{cap}}(t))}{R} \\ &\times e\left(-\frac{R}{a_s}\right), \quad (\text{C1}) \end{aligned}$$

which is the straightforward generalization of the potential used in TDPot [41] for a target with $Z_2 = -1$. It is based on the statistical description of an ion with a positive nucleus (charge Z_1) and surrounding electron cloud (with N_1 electrons) interacting with dynamically screened electrons. The distance between the two nuclei is R ; ϕ and $\phi_{\text{hollow}}^{\text{cap}}$ are particular screening functions discussed below. The first and second terms of Eq. (C1) describe the interaction of the screened part of the projectile's nuclear charge [$Z_1 - q(t) = N_1(t)$] with electrons. The last term is the remaining interaction with the total (unscreened) ion charge $q(t) = Z_1 - N_1(t)$ with target electrons. As in TDPot [41], we used the Krypton-Carbon KrC [53] for the screening function $\phi(x)$. The corresponding screening length is given by [54,55]

$$a_1(N_1, N_2) = \frac{0.8854}{N_1^{0.23} + N_2^{0.23}}, \quad (\text{C2})$$

where $N_2 = (0.8854/a_s)^{-3}$ for dynamically screened electrons, with a_s determined from the plasmon energy.

A neutral atom with many empty inner shells, and consequently many electrons in high- n Rydberg states, is called a hollow atom and forms due to classical-over-barrier charge transport in front of a solid surface [56]. The weakly bound electrons N_{cap} lead to a different screening described by the function $\phi_{\text{hollow}}^{\text{cap}}(R, r_0)$ (see Ref. [41]). r_0 is the critical capture distance for the first electron transfer above the surface, R_c . It is a function of q_{in} and could be determined from the classical-over-barrier model directly [56]. To describe the experiments from Gruber *et al.* [22], we used the following expression:

$$R_c = 3.42 + 3.02\sqrt{q_{\text{in}}}, \quad (\text{C3})$$

determined from TDDFT calculations [22] and differing only little from the result of Burgdörfer *et al.* [56].

- [1] D. Bohm, A suggested interpretation of the quantum theory in terms of “hidden” variables. I, *Phys. Rev.* **85**, 166 (1952).
- [2] D. Bohm, A suggested interpretation of the quantum theory in terms of “hidden” variables. II, *Phys. Rev.* **85**, 180 (1952).
- [3] P. R. Holland, *The Quantum Theory of Motion* (Cambridge University Press, Cambridge, 1993).
- [4] D. Bohm and B. J. Hiley, *The Undivided Universe: An Ontological Interpretation of Quantum Theory* (Routledge, London, 1993).
- [5] D. Dürr, S. Goldstein, and N. Zanghì, Quantum equilibrium and the origin of absolute uncertainty, *J. Stat. Phys.* **67**, 843 (1992).
- [6] R. E. Wyatt, *Quantum Dynamics with Trajectories* (Springer, New York, 2005).
- [7] A. S. Sanz and S. Miret-Artés, *A Trajectory Description of Quantum Processes. I. Fundamentals: A Bohmian Perspective*, Lecture Notes in Physics (Springer Berlin, Heidelberg, 2012).
- [8] A. S. Sanz and S. Miret-Artés, Quantum phase analysis with quantum trajectories: A step towards the creation of a Bohmian thinking, *Am. J. Phys.* **80**, 525 (2012).
- [9] X. Oriols, Quantum trajectory approach to time dependent transport in mesoscopic systems, *Phys. Rev. Lett.* **98**, 066803 (2007).
- [10] R. P. Rundle, T. Tilma, J. H. Samson, V. M. Dwyer, R. F. Bishop, and M. J. Everitt, General approach to quantum mechanics as a statistical theory, *Phys. Rev. A* **99**, 012115 (2019).
- [11] O. Morandi, On the connection between the Wigner and the Bohm quantum formalism, *Phys. Lett. A* **443**, 128223 (2022).
- [12] F. Haas, *Quantum Plasmas: An Hydrodynamic Approach*, Springer Series on Atomic, Optical, and Plasma Physics (Springer, New York, 2011).
- [13] S. Lohmann and D. Primetzhofer, Disparate energy scaling of trajectory-dependent electronic excitations for slow protons and He ions, *Phys. Rev. Lett.* **124**, 096601 (2020).
- [14] X. Qi, F. Bruneval, and I. Maliyov, *Ab initio* prediction of a negative Barkas coefficient for slow protons and antiprotons in LiF, *Phys. Rev. Lett.* **128**, 043401 (2022).
- [15] C. Shepard, D. C. Yost, and Y. Kanai, Electronic excitation response of DNA to high-energy proton radiation in water, *Phys. Rev. Lett.* **130**, 118401 (2023).
- [16] A. Lim, W. M. C. Foulkes, A. P. Horsfield, D. R. Mason, A. Schleife, E. W. Draeger, and A. A. Correa, Electron elevator: Excitations across the band gap via a dynamical gap state, *Phys. Rev. Lett.* **116**, 043201 (2016).
- [17] K. Nordlund, M. Ghaly, R. S. Averback, M. Caturla, T. Diaz de la Rubia, and J. Tarus, Defect production in collision cascades in elemental semiconductors and fcc metals, *Phys. Rev. B* **57**, 7556 (1998).
- [18] M. A. Nastasi, J. W. Mayer, and Y. Wang, *Ion Beam Analysis: Fundamentals and Applications* (CRC Press, Taylor & Francis Group, Boca Raton, 2014).
- [19] R. R. Wilson, Radiological use of fast protons, *Radiology* **47**, 487 (1946).
- [20] Y. T. Zhao, Y. N. Zhang, R. Cheng, B. He, C. L. Liu, X. M. Zhou, Y. Lei, Y. Y. Wang, J. R. Ren, X. Wang, Y. H. Chen, G. Q. Xiao, S. M. Savin, R. Gavrilin, A. A. Golubev, and D. H. H. Hoffmann, Benchmark experiment to prove the role of projectile excited states upon the ion stopping in plasmas, *Phys. Rev. Lett.* **126**, 115001 (2021).
- [21] V. E. Zakharov and S. V. Manakov, On the complete integrability of a nonlinear schrödinger equation, *Theor. Math. Phys.* **19**, 551 (1974).
- [22] E. Gruber, R. A. Wilhelm, R. Pétuya, V. Smejkal, R. Kozubek, A. Hierzenberger, B. C. Bayer, I. Aldazabal, A. K. Kazansky, F. Libisch, A. V. Krasheninnikov, M. Schleberger, S. Facsko, A. G. Borisov, A. Arnau, and F. Aumayr, Ultrafast electronic response of graphene to a strong and localized electric field, *Nat. Commun.* **7**, 13948 (2016).
- [23] A. Niggas, L. Fischer, S. Kretschmer, M. Werl, H. Biber, C. Speckmann, N. McEvoy, J. Kotakoski, F. Aumayr, A. V. Krasheninnikov, and R. A. Wilhelm, Charge-exchange-dependent energy loss of H and He in freestanding monolayers of graphene and MoS₂, *Phys. Rev. A* **108**, 062823 (2023).
- [24] H. Hagstrum, Auger ejection of electrons from tungsten by noble gas ions, *Phys. Rev.* **96**, 325 (1954).
- [25] L. S. Cederbaum, J. Zobeley, and F. Tarantelli, Giant intermolecular decay and fragmentation of clusters, *Phys. Rev. Lett.* **79**, 4778 (1997).
- [26] R. A. Wilhelm, E. Gruber, J. Schwestka, R. Kozubek, T. I. Madeira, J. P. Marques, J. Kobus, A. V. Krasheninnikov, M. Schleberger, and F. Aumayr, Interatomic Coulombic decay: The mechanism for rapid deexcitation of hollow atoms, *Phys. Rev. Lett.* **119**, 103401 (2017).
- [27] P. L. Grande, Bohr’s stopping-power formula derived for a classical free-electron gas, *Phys. Rev. A* **104**, 012807 (2021).
- [28] R. A. Wilhelm, The charge exchange of slow highly charged ions at surfaces unraveled with freestanding 2D materials, *Surf. Sci. Rep.* **77**, 100577 (2022).
- [29] P. Sigmund, *Particle Penetration and Radiation Effects*, 1st ed. (Springer, Berlin, Heidelberg, New York, 2006), Vol. 1, p. 151.
- [30] V. Sharoglazova, M. Puplauskis, C. Mattschas, C. Toebes, and J. Klaers, Energy–speed relationship of quantum particles challenges Bohmian mechanics, *Nature (London)* **643**, 67 (2025).
- [31] J. Lindhard, On the properties of a gas of charged particles, *K. Dan. Vidensk. Selsk. Mat.-Fys. Medd.* **28**, 1 (1954).
- [32] A. Messiah, *Quantum Mechanics* (North-Holland Publishing Company, Amsterdam, 1967), Vol. 1.
- [33] See Supplemental Material at <http://link.aps.org/supplemental/10.1103/7plq-xskx> for additional details, which includes Refs. [57–65].
- [34] I. Nagy and P. M. Echenique, Stopping power of an electron gas for antiprotons at intermediate velocities, *Phys. Rev. A* **47**, 3050 (1993).
- [35] A. F. Lifschitz and N. R. Arista, Velocity-dependent screening in metals, *Phys. Rev. A* **57**, 200 (1998).
- [36] J. C. Ashley, Optical-data model for the stopping power of condensed matter for protons and antiprotons, *J. Phys.: Condens. Matter* **3**, 2741 (1991).
- [37] P. L. Grande, Alternative treatment for the energy-transfer and transport cross section in dressed electron-ion binary collisions, *Phys. Rev. A* **94**, 042704 (2016).
- [38] F. Matias, R. C. Fadanelli, P. L. Grande, N. E. Koval, R. D. Muiño, A. G. Borisov, N. R. Arista, and G. Schiwietz, Ground- and excited-state scattering potentials for the stopping of protons in an electron gas, *J. Phys. B: At. Mol. Opt. Phys.* **50**, 185201 (2017).

- [39] I. Nagy and A. Bergara, A model for the velocity-dependent screening, *Nucl. Instrum. Methods Phys. Res. Sect. B* **115**, 58 (1996).
- [40] M. Quijada, A. G. Borisov, I. Nagy, R. D. Muiño, and P. M. Echenique, Time-dependent density-functional calculation of the stopping power for protons and antiprotons in metals, *Phys. Rev. A* **75**, 042902 (2007).
- [41] R. A. Wilhelm and P. L. Grande, Unraveling energy loss processes of low energy heavy ions in 2D materials, *Commun. Phys.* **2**, 89 (2019).
- [42] A. Niggas, M. Werl, F. Aumayr, and R. A. Wilhelm, Charge exchange of slow highly charged ions from an electron beam ion trap with surfaces and 2D materials, *J. Phys. B: At. Mol. Opt. Phys.* **57**, 072001 (2024).
- [43] J. P. Briand, L. de Billy, P. Charles, S. Essabaa, P. Briand, R. Geller, J. P. Desclaux, S. Bliman, and C. Ristori, Production of hollow atoms by the excitation of highly charged ions in interaction with a metallic surface, *Phys. Rev. Lett.* **65**, 159 (1990).
- [44] M. H. Gass, U. Bangert, A. L. Bleloch, P. Wang, R. R. Nair, and A. K. Geim, Free-standing graphene at atomic resolution, *Nat. Nanotechnol.* **3**, 676 (2008).
- [45] Y. Abe, T. Tanaka, H. Sawada, E. Okunishi, Y. Kondo, Y. Tanishiro, and K. Takayanagi, Electron energy loss spectroscopy of graphene identified by aberration, corrected TEM at 300 kV, *Microsc. Microanal.* **15**, 1484 (2009).
- [46] R. Garcia-Molina, I. Abril, C. D. Denton, and S. Heredia-Avalos, Allotropic effects on the energy loss of swift H^+ and He^+ ion beams through thin foils, *Nucl. Instrum. Methods Phys. Res. Sect. B* **249**, 6 (2006).
- [47] See Supplemental Material of Ref. [22].
- [48] A. Niggas, The role of contaminations in the interaction of highly charged ions with 2D materials, Ph.D. thesis, TU Wien, 2019.
- [49] A. Niggas, S. Creutzburg, J. Schwestka, B. Wockinger, T. Gupta, P. L. Grande, D. Eder, J. P. Marques, B. C. Bayer, F. Aumayr, R. Bennett, and R. A. Wilhelm, Peeling graphite layer by layer reveals the charge exchange dynamics of ions inside a solid, *Commun. Phys.* **4**, 180 (2021).
- [50] Note that for larger scattering angles (i.e., transmission angles) the charge-state-dependent nuclear losses may become significant [41,66].
- [51] <https://doi.org/10.5281/zenodo.18497123>
- [52] J. D. Jackson, *Classical Electrodynamics*, 3rd ed. (John Wiley and Sons, Hoboken, NJ, 1998).
- [53] W. D. Wilson, L. G. Haggmark, and J. P. Biersack, Calculations of nuclear stopping, ranges, and straggling in the low-energy region, *Phys. Rev. B* **15**, 2458 (1977).
- [54] J. Ziegler, J. Biersack, and U. Littmark, *The Stopping and Range of Ions in Solids* (Pergamon Press, New York, 1985).
- [55] R. A. Wilhelm, E. Gruber, V. Smejkal, S. Facsco, and F. Aumayr, Charge-state-dependent energy loss of slow ions. I. Experimental results on the transmission of highly charged ions, *Phys. Rev. A* **93**, 052708 (2016).
- [56] J. Burgdörfer, P. Lerner, and F. W. Meyer, Above-surface neutralization of highly charged ions: The classical over-the-barrier model, *Phys. Rev. A* **44**, 5674 (1991).
- [57] T. Kato, On the eigenfunctions of many-particle systems in quantum mechanics, *Commun. Pure Appl. Math.* **10**, 151 (1957).
- [58] M. Abramowitz and I. A. Stegun, *Handbook of Mathematical Functions with Formulas, Graphs, and Mathematical Tables*, Applied Mathematics Series (U.S. Government Printing Office, Washington, DC, 1972).
- [59] D. R. Penn, Electron mean-free-path calculations using a model dielectric function, *Phys. Rev. B* **35**, 482 (1987).
- [60] M. Vos and P. L. Grande, Extension schemes of the dielectric function, and their implications for ion stopping calculations, *J. Phys. Chem. Solids* **133**, 187 (2019).
- [61] E. Shiles, T. Sasaki, M. Inokuti, and D. Y. Smith, Self-consistency and sum-rule tests in the Kramers-Kronig analysis of optical data: Applications to aluminum, *Phys. Rev. B* **22**, 1612 (1980).
- [62] B. Henke, E. Gullikson, and J. Davis, X-ray interactions: Photoabsorption, scattering, transmission, and reflection at $E = 50\text{--}30,000$ eV, $Z = 1\text{--}92$, *At. Data Nucl. Data Tables* **54**, 181 (1993).
- [63] Z. J. Ding, Ding's microsolid research group, research group webpage (2025), <https://micro.ustc.edu.cn/ELF/Al.html>.
- [64] IAEA Nuclear Data Section, version 2024-11, <https://nds.iaea.org/stopping/>, released 27 November 2024, database maintained by IAEA Nuclear Data Section since 2015, currently compiled by Claudia Montanari.
- [65] P. L. Grande and G. Schiwietz, CasP: Convolution approximation for swift particles (2021), <http://www.casp-program.org>, computer program, freely available.
- [66] R. A. Wilhelm and W. Möller, Charge-state-dependent energy loss of slow ions. II. Statistical atom model, *Phys. Rev. A* **93**, 052709 (2016).